Journal article published in: J. Phys. Chem. A 2014, 118, 1, 152-157
https://pubs.acs.org/doi/10.1021/jp4120749

Nonequilibrium H/D Isotope Effects from Trajectory-based Nonadiabatic Dynamics

Lasse Spörkel, Ganglong Cui,* Axel Koslowski, and Walter Thiel*
Max-Planck-Institut für Kohlenforschung, Kaiser-Wilhelm-Platz 1, 45470, Mülheim an der Ruhr, Germany Received October 2, 2013; E-mail: ganglong@kofo.mpg.de; thiel@kofo.mpg.de

Abstract:

Ground-state equilibrium kinetic isotope effects can be treated well in the framework of transition state theory, whereas excited-state nonequilibrium isotope effects are theoretically less explored. In this letter, we use high-level electronic structure calculations (MS-CASPT2, DFT/MRCI, and TDDFT) and full-dimensional OM2/MRCI-based nonadiabatic dynamics simulations to study the ultrafast intramolecular excited-state proton transfer (ESIPT) and the subsequent deactivation of 7-(2-pyridyl)-indol (7PyIn) and its deuterated analogue (7PyIn-D). We evaluate a total of 1367 surface-hopping trajectories to establish the differences in the dynamical behavior of 7PyIn and 7PyIn-D. The computed H/D isotope effects for ESIPT and excited-state decay are consistent with recent experimental results from femtosecond pump-probe resonance-enhanced multi-photon ionization spectroscopy. We also analyze the influence of temperature fluctuations in the initially prepared sample on the photodynamics of 7PyIn and 7PyIn-D. The present work shows for the first time that trajectory-based nonadiabatic dynamics simulations can capture nonequilibrium H/D isotope effects in excited-state processes.

Proton transfer is ubiquitous in chemical and biological systems and optoelectronic materials, including ion channels of membrane proteins,[1] green fluorescence proteins,[2] natural and synthesized water-oxidation centers,[3,4] light-emitting diodes,[5] and other systems.[6–10] In the past decades, kinetic H/D isotope effects have been measured in numerous experiments to elucidate the detailed mechanism of chemical reactions involving proton or hydrogen transfer. The influence of isotopic substitution on the reaction rate is normally evaluated in the framework of transition state theory.[11] However, such treatment is invalid for ultrafast nonequilibrium processes, e.g. an excited-state intramolecular proton transfer (ESIPT) on an essentially barrierless potential energy surface, because this process is already completed before arriving at its thermodynamic equilibrium. Quantum wavepacket dynamics can be used to simulate ESIPT processes[12] and to analyze excited-state nonequilibrium H/D isotope effects,[13] but such calculations are quite expensive and are thus, at the current stage, limited to model systems with a few degrees of freedom. This bottleneck can be overcome by full-dimensional trajectory-based surface-hopping simulations,[14–16] which have been widely applied in recent years (for reviews see Refs.[17,18]). However, to our knowledge, such dynamics simulations have not yet addressed excited-state nonequilibrium isotope effects.

In this letter, we chose 7-(2-pyridyl)-indole (7PyIn) as our target system to explore ESIPT-related nonequilibrium isotope effects. We use OM2/MRCI-based surface-hopping simulations for this purpose,[16] which have recently been applied successfully to study the excited-state dynamics of medium-sized organic molecules (see, for example, Refs.[2,19–25]). Experimentally,[26] transient absorption (TA) spectra of 7PyIn in solution reveal that the initially excited species decays to the ground state in about 1.0 ps. Femtosecond pump-probe resonance-enhanced multi-photon ionization (REMPI) in a supersonic jet generates an immediate strong ion signal indicating an ultrafast depopulation of the initially generated S_1 species in the gas phase, which has been attributed to ESIPT coupled with a twisting motion, with time constants of 280 fs for 7PyIn and 390 fs for the deuterated analogue.[26] A second small ion signal in the REMPI spectra after about 1 ps has been ten-tatively associated with excited-state decay after one period of a torsional vibrational motion.[26] Previous electronic structure calcu-lations have addressed the photochemical mechanism of 7PyIn in much detail,[27] but complementary dynamical insights remain de-sirable. Therefore, we report the first trajectory-based nonadiabatic dynamics simulations of the photodynamics of 7PyIn and 7PyIn-D. We demonstrate that trajectory-based dynamics simulations are capable of describing the experimentally observed nonequilibrium H/D isotope effects. Furthermore, we perform an initial-condition temperature-decomposition analysis to evaluate the influence of thermal fluctuations on the photoinduced processes. In the following, we summarize our main results; the computational methods and further detailed results are presented in the Supporting Information (SI).

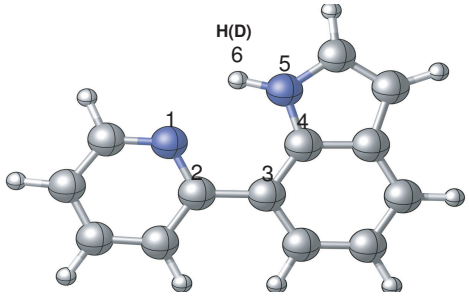

Figure 1. Molecules studied in this work: 7PyIn and its deuterated analogue 7PyIn-D. Color code: nitrogen atoms in blue, carbon atoms in gray, and hydrogen atoms in white. Also shown is the numbering scheme for some relevant atoms.

At the B3LYP/6-31G* level, there are four ground-state minima for 7PyIn, which are referred to as S0-syn, S0-anti, S0-syn-ht, and S0-anti-ht (see Fig. SI-1). The most stable syn conformer (S0-syn, Figure 1) has C_s symmetry and a strong intramolecular hydrogen bond (N5-H6···N1). The anti conformer, S0-anti, is less stable by 5.9 kcal/mol, while the ground-state tautomers generated by transfer of H6 from N5 to N1 (S0-syn-ht and S0-anti-ht) are much higher in energy (see Table SI-2).

The vertical excitation energy to the first singlet excited state of the S0-syn conformer was computed with a variety of elec-tronic structure methods (see Table 1) including time-dependent density functional theory (TD-DFT using the B3LYP, CAM-B3LYP, and M06-2X exchange-correlation functionals), DFT-based multireference configuration interaction (DFT/MRCI), and multi-state complete-active-space second-order perturbation theory (MS-CASPT2). Computation of the full absorption spectrum (see Fig. SI-3) shows that the $S_0 \rightarrow S_1$ electronic transition gives rise to the strongest absorption band. The S_1 state is of partial charge-

Table 1. Calculated $S_0 \rightarrow S_1$ Vertical Excitation Energies (in eV)[a]

Entries	TD-B3LYP[b]	TD-CAM-B3LYP[b]	TD-M062X[b]	OM2/MRCI[c]	DFT/MRCI[d]	MS-CASPT2[e]	RI-CC2[f]
S_1	3.59	4.06	4.08	4.37	3.95	4.34	4.0

[a] See text and SI for description of the methods, see SI for the computed absorption spectrum;
[b] B3LYP/6-31G* optimized structure, energies from single-point TD-DFT/6-31++G** calculations;
[c] OM2/MRCI(12,12) energy at the corresponding optimized structure;
[d] CASSCF(10,8)/6-31G* optimized structure, energy from single-point DFT/MRCI calculation (BHLYP/TZVP);
[e] CASSCF(10,8)/6-31G* optimized structure, energy from single-point MS-CASPT2(14,12)/cc-pVTZ calculation; note that single-point MS-CASPT2(14,12)/6-31G*, MS-CASPT2(10,8)/6-31G*, and MS-CASPT2(10,8)/cc-pVTZ calculations give values of 4.38, 4.69, and 4.48 eV, respectively; the SA3-CASSCF(10,8)/6-31G* value is 5.37 eV;
[f] Coupled cluster RI-CC2/cc-pVDZ result from Sobolewski and Domcke.[27]

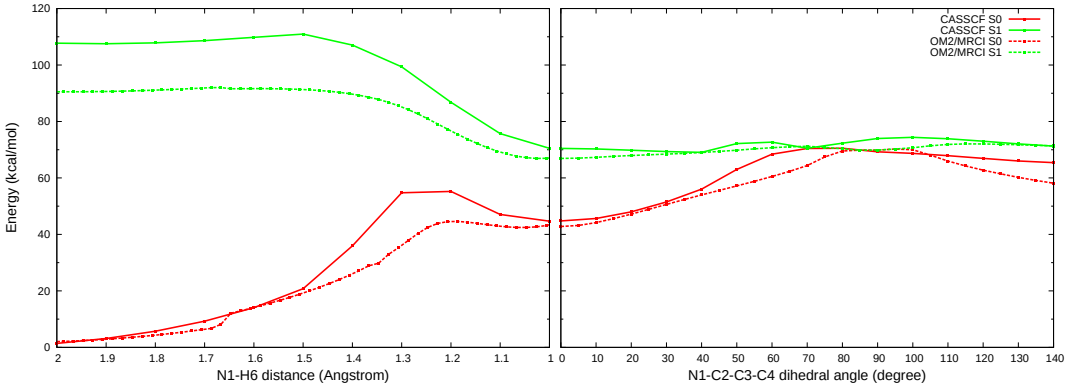

Figure 2. CASSCF/6-31G* and OM2/MRCI energy profiles for relaxed one-dimensional minimum-energy paths (MEPs) along the N1-H6 bond length (left) and the N1-C2-C3-C4 dihedral angle (right). The S_1 MEPs are fully optimized with respect to the other coordinates, while the S_0 curves are obtained from single-point calculations.

transfer character so that the conventional hybrid functional B3LYP underestimates its energy by ca. 0.5 eV, compared with range-separated (CAM-B3LYP) and modern (M06-2X) functionals. The latter give vertical excitation energies (4.06–4.08 eV) that are close to the values from DFT/MRCI (3.95 eV) and the coupled-cluster CC2 method (4.0 eV[27]), but lower than the OM2/MRCI result (4.37 eV) and the MS-CASPT2 results that range between 4.34 and 4.69 eV for different active spaces and basis sets (see Table 1).

In the Franck-Condon (FC) region, we could locate a very shallow S_1 minimum for the syn conformer (S1-syn) at the OM2/MRCI and CASSCF(10,8) levels (see Table SI-2), with very small barriers to tautomerization via ESIPT (see below). This minimum was not obtained in previous RI-CC2/SV(P) calculations that predicted a barrierless ESIPT process.[27] Experimentally, the ESIPT is also believed to be essentially barrierless because lowering the temperature does not stop the ultrafast excited-state deactivation.[26] Our scans of the S_1 minimum-energy ESIPT reaction path (transfer of H6 from N5 to N1) indicate a barrier of 1.5 kcal/mol at the OM2/MRCI level (see Figure 2), which is found to be insignificant in our OM2/MRCI dynamics simulations (see below). The CASSCF/6-31G* energy profiles look qualitatively similar, with a rather flat S_1 plateau in the early ESIPT stages (see Figure 2). Single-point MS-CASPT2/6-31G* calculations at the CASSCF geometries yield an ESIPT barrier of 2.7 kcal/mol in the S_1 state (see Fig. SI-4).

After the transfer of H6, the S_1 potential energy profile of the resulting tautomer is rather flat with regard to the N1-C2-C3-C4 dihedral angle in the whole range between 0° and 90° (see Figure 2). This twist leads to the S_1/S_0 conical intersection region. We have optimized the minimum-energy S_1/S_0 conical intersection (MECI, labeled as S1S0-CI). Its N1-C2-C3-C4 dihedral angle is computed to be 63.2° at the CASSCF(10,8)/6-31G* level, close to the recent CASSCF(6,6)/6-31G* optimized value of 72°,[28] but considerably smaller than the RI-CC2/SV(P) estimate of ca. 90°.[27] OM2/MRCI yields a rather extended and flat conical intersection region for N1-C2-C3-C4 dihedral angles between 50° and 90°, with an essentially perpendicular MECI (like RI-CC2, see SI for further detailed information). Energetically, this conical intersection is easily accessed: the energy gap relative to the most stable S_0 syn conformer is computed to be 3.37 eV at the MS-CASPT2 level and 3.35 eV at the OM2/MRCI level; these values are considerably lower than the corresponding S_1 vertical excitation energies of 4.69 and 4.37 eV at the FC point. The computed relaxed potential energy profiles (Figure 2) suggest that the dynamics from the FC region to S1S0-CI should be very fast (as confirmed by our OM2/MRCI simulations, see below). Single-point MS-CASPT2/6-31G* calculations at the CASSCF geometries also give a rather flat profile, but there remains a sizable S_0/S_1 energy gap in the MECI region because of the use of CASSCF geometries (see Fig. SI-4).

To gain further insight into the dynamics, we performed extensive full-dimensional nonadiabatic surface-hopping simulations, with a total of 632 trajectories for 7PyIn and 735 for 7PyIn-D (2 ps each, see SI for details of the simulations and their analysis). Our main focus is the nonequilibrium H/D isotope effect on the ultrafast ESIPT process of 7PyIn. We adopted the criterion to measure the ESIPT time in each trajectory at the point when the distance in the breaking N5-H6 bond exceeds 1.5 Å, which yields average ESIPT times of 274 fs for 7PyIn and 339 fs for 7PyIn-D (see Fig. SI-7 and the associated discussion). These values are consistent with the spectroscopically observed H/D isotope effect: As mentioned above, Nosenko *et al.*[26] attributed the first ion signal in pump-probe REMPI spectra to the ESIPT process and determined time constants of 280 fs for 7PyIn and 390 fs for 7PyIn-D in a supersonic jet (for depopulation of the initially excited species by ESIPT[29]). Moreover, their second small ion signal at about 1.0 ps may correspond to the few ESIPT events observed in our simulations in this range, especially for 7PyIn-D (see Figure 3). In spite of lacking nuclear

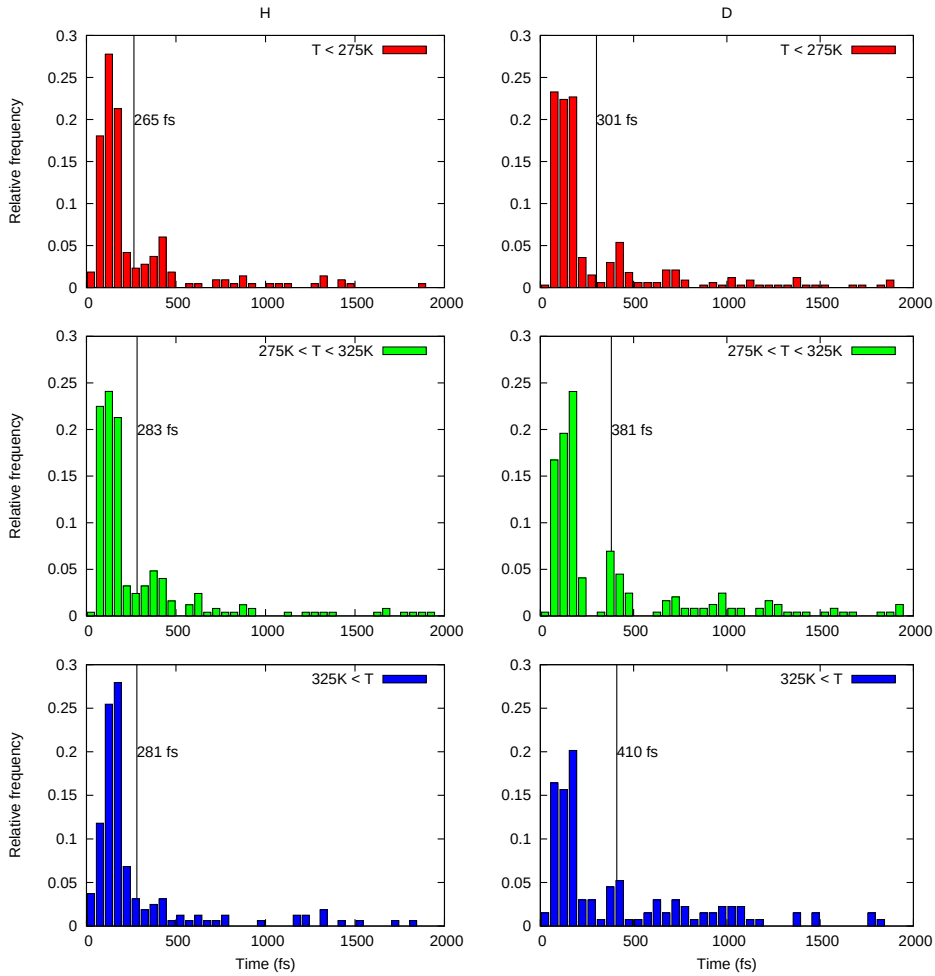

Figure 3. ESIPT time distributions in three temperature windows of initial conditions (top: less than 275 K; middle: between 275 and 325 K; bottom: greater than 325 K).

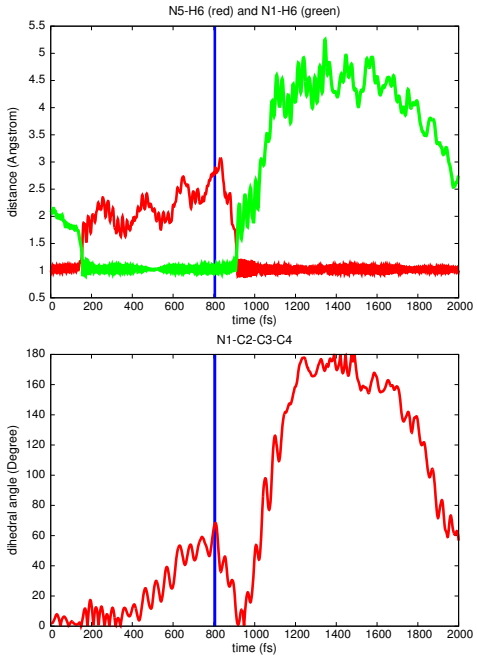

Figure 4. A typical trajectory for 7PyIn. The excited-state proton transfer is completed at 200 fs and after another 600 fs, the $S_1 \rightarrow S_0$ internal conversion takes place. In the S_0 state, the hydrogen atom is transferred back to the original donor atom. See text for more details.

quantum effects, trajectory-based dynamics simulations thus seem capable of capturing nonequilibrium H/D isotope effects, in particular for essentially barrierless ultrafast processes such as ESIPT.

We have further analyzed the influence of thermal fluctuations in the initially prepared ensemble on the ESIPT time distribution (see Figure 3). Overall, the higher the temperature, the longer the ESIPT time. This can be understood in a qualitative manner. A higher temperature implies a higher kinetic energy, which is reflected in nuclear motions that sample distorted molecular geometries further away from the ground-state equilibrium structure. In the case of 7PyIn, the planar ground-state structure contains a nearly "perfect" hydrogen-bonding arrangement, which is ideally suited for ESIPT after vertical excitation. On the other hand, the ESIPT process will be less favorable (and thus take longer) when the vertical excitation occurs from distorted structures, especially those with strong out-of-plane displacements, which will be encountered more often at higher temperatures. In our simulations, this is reflected in average ESIPT times that increase with increasing temperature in the three chosen windows (7PyIn from 265 fs to 283 and 281 fs, 7PyIn-D from 301 fs to 381 and 410 fs).

The average hopping time in our trajectories is found to be 605 fs for 7PyIn and 669 fs for 7PyIn-D (see Fig. SI-8), indicating that internal conversion occurs about 330 fs after completion of the ESIPT process. Both isotopomers thus take roughly the same time for the twisting motion that is required to reach the conical intersection region. The computed gas-phase excited-state decay times

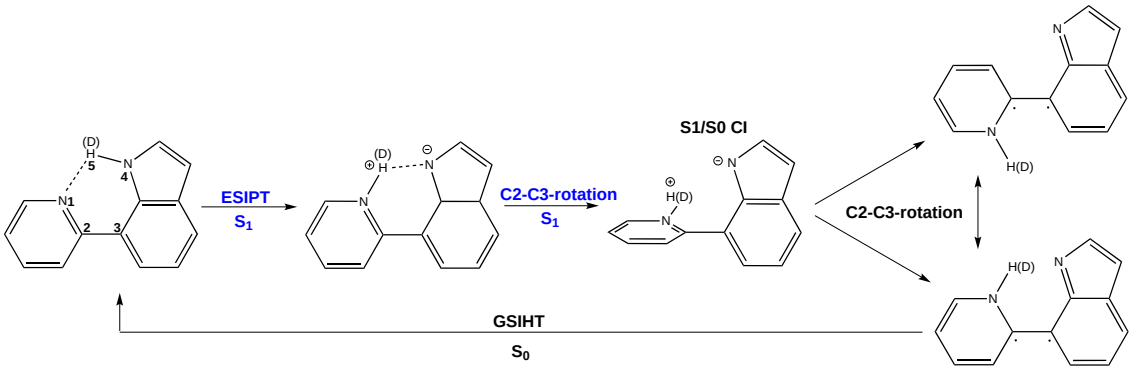

Figure 5. Proposed photochemical mechanism for 7PyIn. An ultrafast ESIPT process is followed by a N1-C2-C3-C4 twist that guides the system toward the conical intersection and allows internal conversion to the S_0 state (see text for details).

and the measured gas-phase REMPI time constants are shorter than excited-state decay time of about 1.0 ps deduced from the TA spectra in solution. Our simulations support the qualitative explanation given previously,[26] namely that the solvent environment may slow down the excited-state deactivation. Access to the S_1/S_0 conical intersection with an N1-C2-C3-C4 dihedral angle of ca. 90° (OM2/MRCI and CC2) requires a twist around the central C2-C3 bond, which will be harder to achieve in solution than in vacuo, because solute-solvent interactions will hinder the required out-of-plane motions.

To illustrate the photodynamics of 7PyIn and to highlight the main photochemical events, we discuss the time evolution of three key geometric parameters in a typical trajectory (see Figure 4). In the first 180 fs after the vertical photoexcitation, the H6 atom remains bound to the N5 atom. During this period, the excited-state decay is impossible because of the very large S_1-S_0 energy gap (more than 80 kcal/mol) and the small S_1/S_0 nonadiabatic coupling. The ESIPT process after ca. 180 fs generates the planar S_1 synht tautomer with an N1-H6$\cdots$N5 hydrogen bond. After roaming around this planar conformation for about 200 fs, the N1-C2-C3-C4 dihedral angle starts to twist, and the molecule then decays to the ground state via the S_1/S_0 conical intersection at 800 fs. At this point, the nonadiabatic coupling is much larger (see Fig. SI-11). After further 100 fs of roaming in the S_0 state, the H6 atom returns back to N5 forming the most stable S0-syn tautomer. Similar dynamical features are observed for the deuterated analogue, albeit with some time delay (see Fig. SI-12 and the associated discussion).

To summarize, we have explored the photodynamics of 7PyIn and its deuterated analogue by means of high-level electronic structure calculations (MS-CASPT2, TDDFT, and DFT/MRCI) and extensive OM2/MRCI nonadiabatic dynamics simulations (1367 successful runs in total). The latter provide mechanistic insights complementary to those from previous electronic structure calculations. We have demonstrated for the first time that full-dimensional trajectory-based dynamics methods are capable of simulating the nonequilibrium H/D isotope effect quite well, despite missing nuclear quantum effects such as tunneling, which should however be unimportant for the essentially barrierless ESIPT processes. We have also analyzed the influence of the thermal fluctuations in the initially prepared sample on the photodynamics of 7PyIn and 7PyIn-D. The current study thus extends the use of trajectory-based nonadiabatic dynamics simulation methods to the study of nonequilibrium H/D isotope effects and temperature effects in ultrafast excited-state processes.

Acknowledgement G.L. thanks the Alexander von Humboldt foundation for a fellowship.

Supporting Information Available: Computational details, further OM2/MRCI validation, additional plots and tables, and Cartesian coordinates of all optimized structures. This material is available free of charge via the Internet at http://pubs.acs.org/.

References

(1) Lórenz-Fonfría, V.; Resler, T.; Krause, N.; Nack, M.; Gossing, M.; von Mollard, G.; Bamann, C.; Bamberg, E.; Schlesinger, R.; Heberle, J. *Proc. Nat. Acad. Sci. U.S.A.* **2013**, *110*, 1273–1281.
(2) Cui, G.; Lan, Z.; Thiel, W. *J. Am. Chem. Soc.* **2012**, *134*, 1662–1672.
(3) Pantazis, D.; Ames, W.; Cox, N.; Lubitz, W.; Neese, F. *Angew. Chem. Int. Ed.* **2012**, *51*, 9935–9940.
(4) Lin, X.; Hu, X.; Concepcion, J.; Chen, Z.; Liu, S.; Meyer, T.; Yang, W. *Proc. Nat. Acad. Sci. U.S.A.* **2012**, *109*, 15669–15672.
(5) Tang, K.; Chang, M.; Lin, T.; Pan, H.; Fang, T.; Chen, K.; Hung, W.; Hsu, Y.; Chou, P. *J. Am. Chem. Soc.* **2011**, *133*, 17738–17745.
(6) Migani, A.; Bearpark, M.; Olivucci, M.; Robb, M. *J. Am. Chem. Soc.* **2007**, *129*, 3703–3713.
(7) Migani, A.; Blancafort, L.; Robb, M.; DeBellis, A. *J. Am. Chem. Soc.* **2008**, *130*, 6932–6933.
(8) Shemesh, D.; Sobolewski, A.; Domcke, W. *J. Am. Chem. Soc.* **2009**, *131*, 1374–1375.
(9) Li, X.; Chung, L.; Mizuno, H.; Miyawaki, A.; Morokuma, K. *J. Phys. Chem. Lett.* **2010**, *1*, 3328–3333.
(10) Hammes-Schiffer, S. *J. Phys. Chem. Lett.* **2011**, *2*, 1410–1416.
(11) Pu, J.; Gao, J.; Truhlar, D. *Chem. Rev.* **2006**, *106*, 3140–3169.
(12) Lan, Z.; Frutos, L.; Sobolewski, A.; Domcke, W. *Proc. Nat. Acad. Sci. U.S.A.* **2008**, *105*, 12707–12712.
(13) Venkataraman, C.; Soudackov, A.; Hammes-Schiffer, S. *J. Chem. Phys.* **2009**, *131*, 154502.
(14) Tully, J. *J. Chem. Phys.* **1990**, *93*, 1061–1071.
(15) Hammes-Schiffer, S.; Tully, J. *J. Chem. Phys.* **1994**, *101*, 4657–4667.
(16) Fabiano, E.; Keal, T.; Thiel, W. *Chem. Phys.* **2008**, *349*, 334–347.
(17) Barbatti, M. *WIREs Comput. Mol. Sci.* **2011**, *1*, 620–633.
(18) Curchod, B.; Rothlisberger, U.; Tavernelli, I. *ChemPhysChem* **2013**, *14*, 1314–1340.
(19) Lan, Z.; Fabiano, E.; Thiel, W. *J. Phys. Chem. B* **2009**, *113*, 3548–3555.
(20) Lu, Y.; Lan, Z.; Thiel, W. *Angew. Chem. Int. Ed.* **2011**, *50*, 6864–6867.
(21) Weingart, O.; Lan, Z.; Koslowski, A.; Thiel, W. *J. Phys. Chem. Lett.* **2011**, *2*, 1506–1509.
(22) Kazaryan, A.; Lan, Z.; Schäfer, L.; Thiel, W.; Filatov, M. *J. Chem. Theory Comput.* **2011**, *7*, 2189–2199.
(23) Cui, G.; Thiel, W. *Angew. Chem. Int. Ed.* **2013**, *52*, 433–436.
(24) Spörkel, L.; Cui, G.; Thiel, W. *J. Phys. Chem. A* **2013**, *117*, 4574–4583.
(25) Gamez, J.; Weingart, O.; Koslowski, A.; Thiel, W. *Phys. Chem. Chem. Phys.* **2013**, *15*, 11814–11821.
(26) Nosenko, Y.; Wiosna-Sałyga, G.; Kunitski, M.; Petkova, I.; Singh, A.; Buma, W.; Thummel, R.; Brutschy, B.; Waluk, J. *Angew. Chem. Int. Ed.* **2008**, *47*, 6037–6040.
(27) Sobolewski, A.; Domcke, W. *J. Phys. Chem. A* **2007**, *111*, 11725–11735.
(28) Kochman, M.; Morrison, C. *J. Chem. Theory Comput.* **2013**, *9*, 1182–1192.
(29) Brutschy, B. private communication. August 2013.